RESEARCH ARTICLE

NANO · MICRO small
www.small-journal.com

Hydrosilylation Adducts to Produce Wide-Temperature Flexible Polysiloxane Aerogel under Ambient Temperature and Pressure Drying

*Bi-Fan Guo, Ye-Jun Wang, Zhang-Hao Qu, Fan Yang, Yu-Qing Qin, Yang Li, Guo-Dong Zhang, Jie-Feng Gao, Yongqian Shi, Pingan Song, and Long-Cheng Tang**

Despite incorporation of organic groups into silica-based aerogels to enhance their mechanical flexibility, the wide temperature reliability of the modified silicone aerogel is inevitably degraded. Therefore, facile synthesis of soft silicone aerogels with wide-temperature stability remains challenging. Herein, novel silicone aerogels containing a high content of Si are reported by using polydimethylvinylsiloxane (PDMVS), a hydrosilylation adduct with water-repellent groups, as a "flexible chain segment" embedded within the aerogel network. The poly(2-dimethoxymethylsilyl)ethylmethylvinylsiloxane (PDEMSEMVS) aerogel is fabricated through a cost-effective ambient temperature/pressure drying process. The optimized aerogel exhibits exceptional performance, such as ultra-low density (50 mg cm^{-3}), wide-temperature mechanical flexibility, and super-hydrophobicity, in comparison to the previous polysiloxane aerogels. A significant reduction in the density of these aerogels is achieved while maintaining a high crosslinking density by synthesizing gel networks with well-defined macromolecules through hydrolytic polycondensation crosslinking of PDEMSEMVS. Notably, the pore/nanoparticle size of aerogels can be fine-tuned by optimizing the gel solvent type. The as-prepared silicone aerogels demonstrate selective absorption, efficient oil–water separation, and excellent thermal insulation properties, showing promising applications in oil/water separation and thermal protection.

1. Introduction

Due to a continuous 3D network structure comprising a hierarchy of hierarchical pores with micro-/nano-sizes, aerogel has many superior properties, for example, high specific surface area, high porosity, low density, and low thermal conductivity, which is found in growing applications such as thermal insulators, superabsorbents, and supports for catalysis.[1–9] Silica-based aerogels obtained through sol–gel polymerization of alkoxysilanes in dilute solvent exhibit ultra-low density and good stability in high or low temperatures owing to the Si—O—Si bond with high bonding energy, attracting great interest.[10] To date, commercial silica aerogels are widely used as efficient thermal insulation materials when space is limited, especially for building and industrial insulation with a rapidly growing market. Unfortunately, although silica aerogels have an excellent strength-to-weight ratio, their brittleness nature and complex fabricating process restrict their large-scale applications. Typically, commercial silica-based aerogels, based mainly

B.-F. Guo, Y.-J. Wang, Z.-H. Qu, F. Yang, Y.-Q. Qin, Y. Li, G.-D. Zhang, L.-C. Tang
College of Material
Chemistry and Chemical Engineering
Key Laboratory of Organosilicon Chemistry and Material Technology of MoE
Key Laboratory of Silicone Materials Technology of Zhejiang Province
Hangzhou Normal University
Hangzhou 311121, China
E-mail: lctang@hznu.edu.cn

J.-F. Gao
School of Chemistry and Chemical Engineering
Yangzhou University
Yangzhou 225002, China

Y. Shi
College of Environment and Safety Engineering
Fuzhou University
Fuzhou 350116, China

P. Song
Centre for Future Materials
University of Southern Queensland
Springfield Campus, QLD 4300, Australia

P. Song
School of Agriculture and Environmental Science
University of Southern Queensland
Springfield, QLD 4300, Australia

The ORCID identification number(s) for the author(s) of this article can be found under https://doi.org/10.1002/smll.202309272

DOI: 10.1002/smll.202309272

on tetraethyl orthosilicate or sodium silicate as the basic raw materials, are fabricated after sol–gel, aging, and drying processes.[11,12] In some cases, silica-based aerogels need expensive drying processes (e.g., CO_2 supercritical drying and freeze drying), making them undesirable for large-scale bulk quantities. Further, the highly cross-linked silica network shows poor mechanical reliability due to their intrinsically fragile/brittle structure constructed by "silica particles," which restrict them from long-term stable thermal insulation.[13–16]

To overcome the brittleness of silica-based aerogels, many exciting efforts have been designed and developed such as i) a silica-based network combined with a flexible polymer network without forming chemical bonds between two networks defined bi-component strategy[15] and ii) introducing low surface energy groups in the aerogel network defined homo-component strategy.[17,18] The reinforced silica-based aerogel obtained via cross-linking with organic compounds, as far, is frequently reported because it shows excellent mechanical properties due to a dual-network structure comprising a "silica particle" framework and polymer chains (e.g., cellulose,[4] polyimide,[19] and alginate).[20] However, the high-performance aerogel obtained by this method usually requires freeze-drying in high-precision instruments. In general, this way only is applied in laboratories to fabricate small-scale samples due to the expensive fees incurred the freeze drying and the high solvent removal rate, limiting the development of its industrialization direction. On the other hand, aerogels with organic–inorganic hybrid networks are prepared using silicone with hydrophobic groups replacing part of the TEOS or sodium silicate as the basic raw materials.[21,22] The homo-component aerogels exhibit better hydrophobicity due to low surface energy groups (e.g., methyl, vinyl, phenyl, sulphydryl, or carbon chains) on the network surface and micro-/nano-porous structure, and some of them have a good absorption capability for organic solvents/oils.[7,23–27] However, the density and wide-temperature mechanical stability of aerogels are yet to be unsatisfactory. Normally, compared with the ultralow molar ratio of the pendant group to the Si—O—Si group (referred to as C/Si ratio) in an aerogel system, the presence of considerable organic groups usually causes a higher C/Si ratio (typically >3) in the final aerogels with a low pyrolysis temperature,[23,26] inducing inevitably poor mechanical reliability under high-temperature environments. Therefore, the design and development of high-performance silicone aerogels combined with ultra-lightweight features and wide-temperature mechanical flexibility with a low C/Si ratio via a cost-effective fabricating process remains a big challenge.

In our recent work, adjusting the low ratio of the pendant group to Si—O—Si groups (i.e., C/Si ratios of 1–2) in silicone resins produces high-temperature tolerant materials that can be applied as green flame-retardant coating on various combustible substrates.[28,29] However, silicone resin materials typically lack mechanical flexibility due to the highly crosslinked network in the final product. Additionally, hydrosilylation is a highly selective reaction without altering the C/Si ratio (≈2) of the silicone rubber system, which was employed to fabricate silicone rubber foam with excellent wide-temperature mechanical flexibility.[30] Inspired by the above silicone chemistry features, herein, we report new organic–inorganic aerogels based on poly(2-dimethoxymethylsilyl)ethylmethylvinyl siloxane (PDEMSEMVS) with a relatively high content of Si element (C/Si ratio of 2–2.2) toward exceptional physical properties, such as wide-temperature flexibility and ultra-low density and multiple functionalities, comprising thermal insulation and selective absorption. The bottle-brush polydimethylvinylsiloxane macromolecules, obtained by the grafting reaction between a single precursor and organoalkoxysilane, are followed with tetramethylammonium hydroxide (TMAOH) as a base catalyst to give an organic–inorganic silicon network structure including flexible PDMVS chains and "SiO_2" units by hydrolytic polycondensation. Aerogels based on the PDEMSEMVS network are prepared using a low-cost ambient temperature and pressure drying (ATPD) process, and their porous nanostructure is readily controlled. Meanwhile, the fabricated approach of each step is discussed from the viewpoint of properties of the chemical group and material structure, showing promising facile fabrication of ultra-lightweight and wide-temperature flexible silicone aerogels for multifunctional applications in complex environments.

2. Results and Discussion

The detailed synthesis procedure of PDEMSEMVS-based aerogel with an organic–inorganic double network is outlined in Supporting information and **Figure 1** for a schematic representation. To address the brittleness of silica aerogel, the bottle-brush PDMVS modified by grafting PDMVS with a flexible chain is dissolved in a mixture containing the binary solvents (BzOH/toluene), TMAOH, and H_2O. Notably, hydrosilylation adducts were employed to synthesize the PDEMSEMVS with a relatively high content of Si element to obtain wide-temperature flexibility. Furthermore, the above solution is aged at 80 °C, leading to the condensation of PDEMSEMVS and the formation of an orange transparent gel (Figure 1a). The obtained gel is washed successively with isopropanol and *n*-hexane to remove residual water and unreacted species, thereby reducing the surface tension in the network, which allows the direct use of the ATPD process. Typically, by using natural environments at ≈25 °C and 1 atm (Movie S1, Supporting Information), a lightweight (≈50 mg cm^{-3}), mechanical flexibility, and super-hydrophobic aerogel, supported by the stamen (Figure 1b), can be successfully fabricated, which is hardly obtained in previous silicone aerogel systems.[10,16,23,24,31,32]

2.1. Chemical Structure and Microstructure

The precursor synthesis was carried out in two steps using a multi-vinyl functional PDMS (PDMVS) intermediate, as shown in Figure 1a. The parameters of time, temperature, and SCR concentration in the ring-opening polymerization are fixed at 5 h, 80 °C, and 5 wt% (Figure S1, Supporting Information). The results on the co-polymerization of D_4 and D_4^{vi} with a ratio of 3:2 or 9:1 can be found in Table S1 and Figure S2, Supporting Information. The successful synthesis of PDMVS is confirmed by ^1H NMR (vinyl and methyl groups observed at 5.96 and 0.15 ppm, respectively) and GPC analysis, and the resulting PDMVS exhibits low dispersity (≈1.8) (Figure S2, Supporting Information). The PDMVS is designed to have a fixed molecular weight to provide flexibility to the eventual aerogel sample (Table S1, Supporting

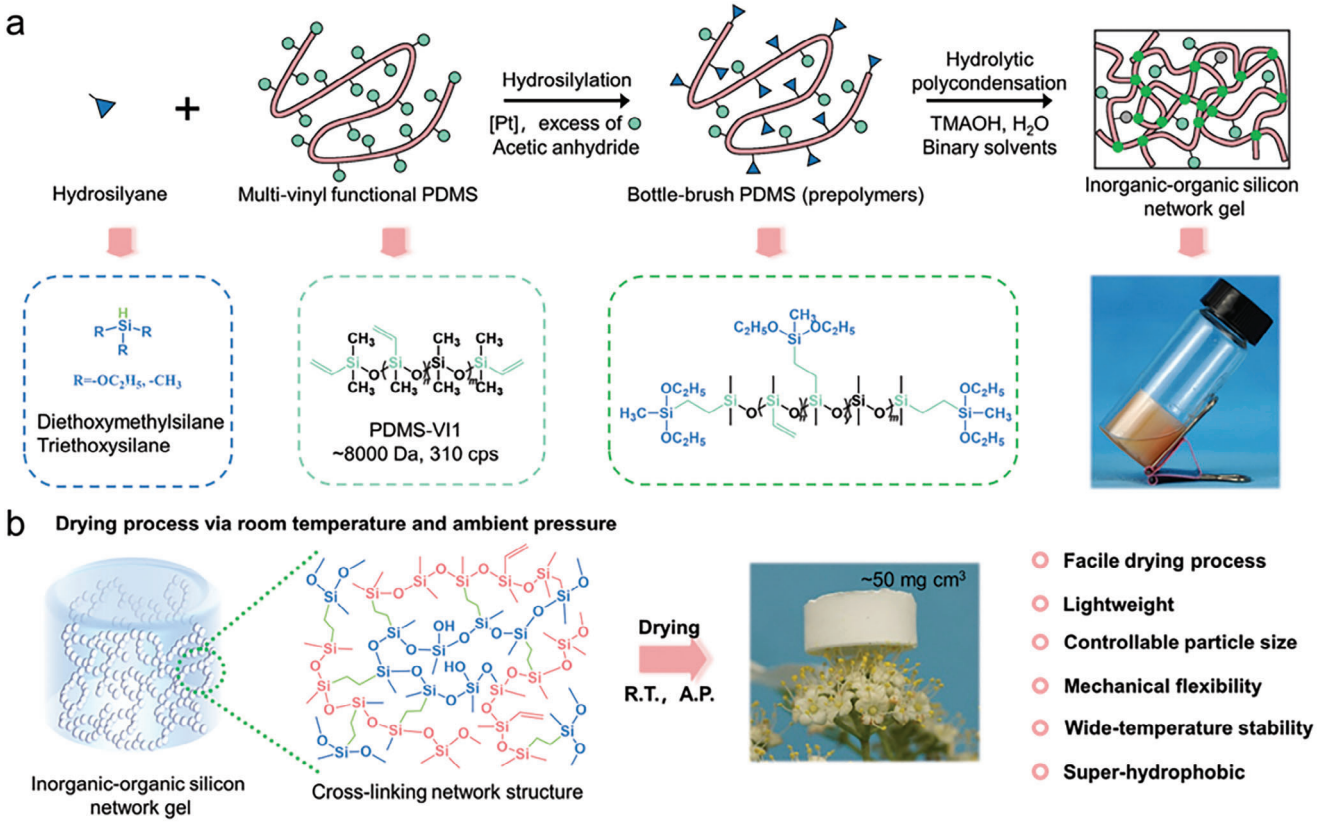

Figure 1. The facile synthesis of ultra-light organic–inorganic silicone aerogel via the hydrosilylation/hydrolytic polycondensation. a) Schematic illustration of the preparation process of wet gel. b) Schematic of aerogel drying process with room temperature and ambient pressure.

Information). Additionally, platinum-catalyzed hydrosilylation, a well-known, robust, and efficient coupling reaction between a vinyl group and a hydrosilane, is selected to graft silicone onto the PDMVS. Considering the reaction rate and subsequent solubility of the precursor and the gel solvent (Table S2, Supporting Information), the molar ratio between —CH=CH_2 and Si—H is fixed at 1:0.6 in the hydrosilylation.

^{1}H NMR, ^{29}Si NMR, and FTIR spectroscopy were employed to further confirm the chemical structure of adducts from the control group (PDMVS-2 and DEMS) (Table S6, Supporting Information). Table S5, Supporting Information, presents the Mn values of adducts, which increase from 11 243 to 17 721 under these conditions. The PDI of adducts exhibits a consistent trend, which can be attributed to the presence of residual small molecules in the system that do not affect subsequent reactions. **Figure** 2a and Figures S3 and S4, Supporting Information, illustrate the chemical shift of hydrogen at different regions: 0.05–0.19, ≈1.22/≈3.7, 4.55, and 5.92 ppm, corresponding to —CH_3, —OCCH and —OCHC, Si—H, and —CH=CH_2, respectively. The ethylene hydrogens within the silethylene structure are observed at ≈0.46 ppm, indicating the occurrence of hydrosilylation between Si—CH=CH_2 and Si—H, achieving a conversion rate of 78.11%. Due to the steric hindrance of adjacent groups, the relative integral area of Si—H and Si—CH=CH to the unchanged area of Si—O—Si decreases respectively from 4.187 to 2.020 and from 2.091 to 0.806, further providing evidence in FTIR (Figure 2b). It should be noted that the system still contains traces of the Si—H group (Figure 2b), which does not impact subsequent steps.

Figure 2c illustrates two new peaks at −4.33 and −5.37 ppm, assigned to $CH_3(CH_3CH_2O)_2$—*Si—CH_2CH_2—Si(—CH_3) and $CH_3(CH_3CH_2O)_2$—*Si—CH_2CH_2—Si(—$CH_3)_2$,[33] respectively. Due to the greater reactivity of end groups to side groups for long chain molecule (precursor), the peak at −3.11 ppm (—*Si(—$CH_3)_2$—CH=CH_2) disappears in the spectrum of the PDMVS-2, indicating the efficient conversion of —*Si(—CH_3)—$CHCH_2$. In addition, the peaks at −20.84/−21.29 and −34.43/34.98/−35.37, corresponding to *Si(—$CH_3)_2$ and Si(—CH=CH_2)—CH_3, are shifted to lower chemical shift: −21.32/−21.84/−22.35 and −35.10/−35.53/−35.97,[34–37] respectively (Figure 2c and Table S6, Supporting Information). These shifts can be attributed to a change in the chemical environment of the Si atom caused by the transformation of conjoint Si—$CHCH_2$ into Si—CH_2CH_2—Si.

In contrast to the aerogels obtained through freeze drying, polysiloxane aerogel requires a solid skeleton or low surface tension in the system. Therefore, optimization of the graft group (hydrosilane) and gel solvent is crucial to control the hydrolysis and polycondensation of DEMSEMVS (precursor) and to produce well-shaped and soft PDEMSEMVS aerogels using the drying technology at ambient temperature and pressure. To achieve low surface energy in the aerogels, the wet gel network contains numerous organic groups, which prevent shrinkage during the drying process from the change of the aerogel's shape.

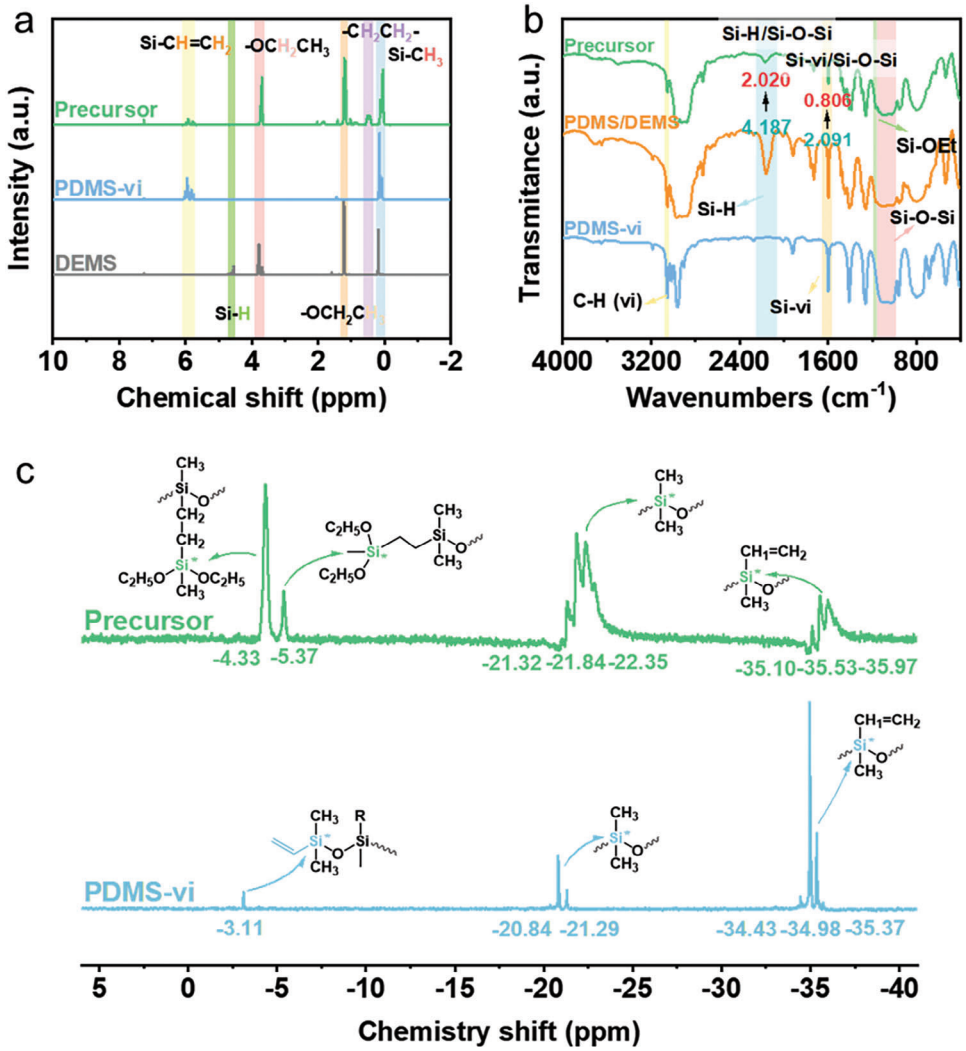

Figure 2. Chemical structure of precursor. a) ^{1}H NMR spectra of DEMS, PMDVS, and precursor. b) FTIR spectra of PMDVS, PMDS/DEMS mixture without Pt catalyzer, and precursor. c) ^{29}Si NMR spectra of PMDVS and precursor.

Therefore, the parameters of the hydrosilane (type and molar ratio) are optimized and selected, as shown in Table S4, Supporting Information. Group 7 exhibits greater softness compared to other groups (Figure S5, Supporting Information) due to the presence of numerous organic groups, such as —CH_3 and —CH_2CH_2, attached to the silicone precursor. Absorption bands corresponding to C—H and Si—C bonds, evident in FTIR and XPS spectra (Figure S6, Supporting Information), further indicate the presence of organic groups. Although a small number of Si—OH groups are present in the resulting network of PDEMSEMVS aerogels (Figure S6a, Supporting Information), most of them undergo transformation into Si—O—Si in the presence of TMAOH. The XPS Si 2p spectra reveal that the intensity of the Si—OH peak, located at ≈102.9 eV, is much weaker compared to the Si—O—Si and Si—C peaks (Figure S6d, Supporting Information). The PDEMSEMVS aerogels exhibit good super-hydrophobicity (see Figure 5), which is advantageous for obtaining well-shaped aerogels from wet gel under ambient temperature and pressure.

Most flexible silica-based aerogels obtained by ambient pressure drying usually exhibit a higher density of over 120 mg cm^{-3} (see Table S8, Supporting Information),[23,26,27] which is attributed to the construction of a tough gel network that resists surface tension caused by solvent evaporation. Recent studies have proposed two strategies to fabricate lower-density aerogels. For example, the C—S bonded with lower bond energy binding for the vacuum drying technology, while semi-crystalline chains were formed under the supercritical s-CO_2 drying technology.[24,38] In this work, we proposed a new approach where a binary solvents (toluene/BzOH mixture) were used as the gel solution to manage the gelation and obtain ultra-lightweight PDEMSEMVS aerogels. As shown in SEM images (**Figure 3a–d**), the aerogels reveal a trend in the resulting PDEMSEMVS aerogels, where the size of "SiO_2" particles decreases gradually and the density of aerogels decreases with an increase in the content of toluene in the gel solution under specific conditions (see Table S7, Supporting Information). Additionally, the A3 aerogel exhibits the best shape and the smallest "SiO_2"

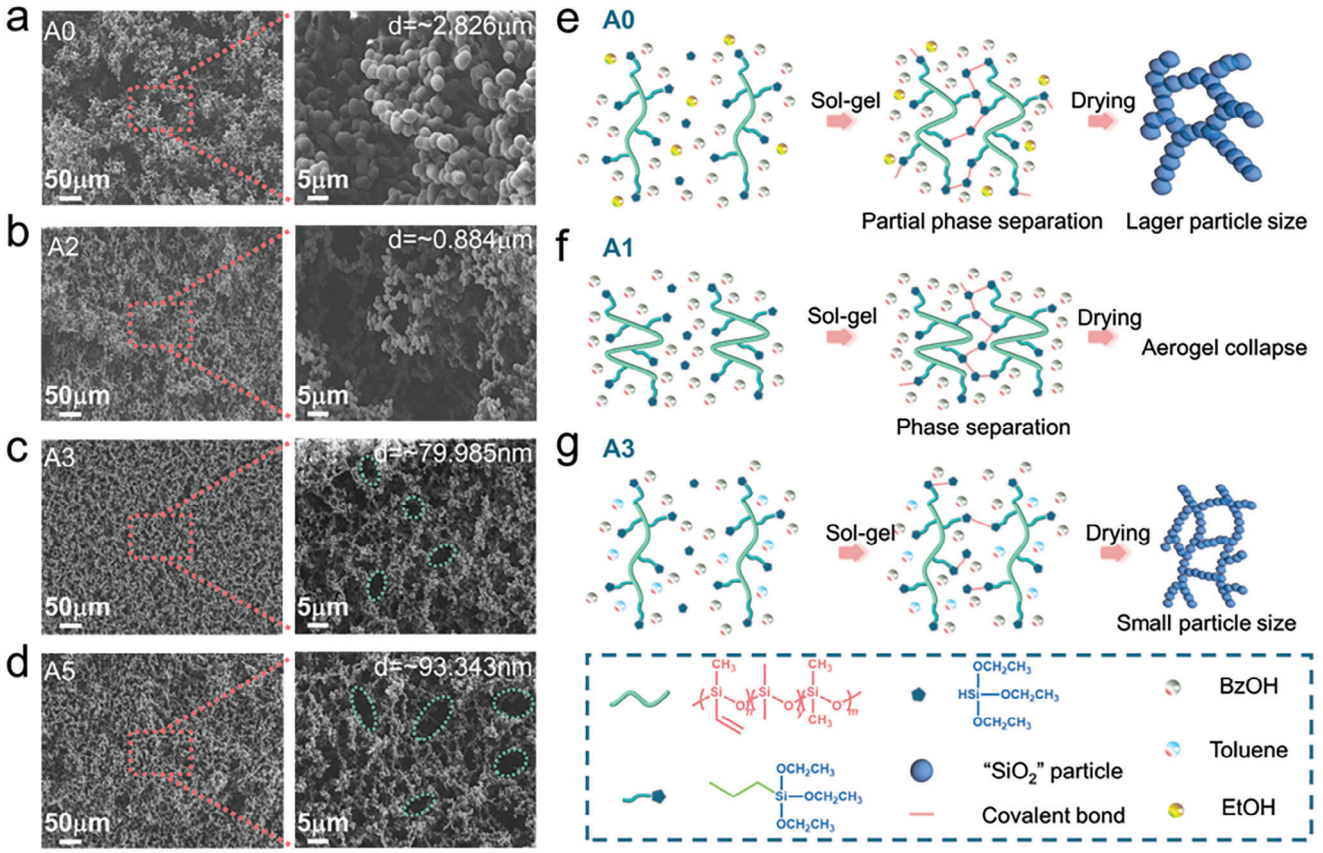

Figure 3. Structure characterization and solvent affect analysis. a–d) SEM images of various aerogels, showing tunable pore structure and morphology, as well as particle sizes. e–g) Schematic illustration of gelation and drying processes to obtain the various pore morphology by adjusting different compositions of solvents.

particle size, ≈78 nm, as shown in Figures S7 and S8, Supporting Information. To gain further insights into these observations, we track and monitor the entire gelation process of three groups (A0, A1, and A3, corresponding to EtOH/BzOH, BzOH, and toluene/BzOH) (see Figure S9, Supporting Information). It is evident that both the A0 and A3 groups turned transparent after being placed in an 80 °C oven, while the A1 remained turbid due to the poor compatibility between BzOH and the precursor. Therefore, using only BzOH as a gel solvent is unsuitable for our aerogel system. Hence, a binary solvent (e.g., A1 and A3) was chosen as a gel solvent to promote the stretching of the precursor with a high molecular weight and achieve a homogeneous mixture based on similar compatibility principle, such as —OCH_2CH_3 group of the precursor and —OH group of EtOH, as well as the organic groups of the precursor and toluene. Moreover, gelation occurs later in the A3 group (at 80 min) compared to that observed in the A1 group (at 52 min) (Figure S9a–e, Supporting Information), suggesting that the non-polar solvent slows down gelation by delaying macroscopic phase separation, which would attributed to intermolecular forces between the toluene and the organic groups of the precursor (Figure 3e–g). Finally, the A3 control group formed a complete gel, while A1 and A0 initially demonstrated solid-liquid separation phenomena (Figure S7f, Supporting Information). Thus, the A3 aerogel exhibits a good shape, small particle size (≈80 nm), small pores, and ultra-low density (≈50 mg cm^{-3}). It is worth noting that increasing the content of toluene in a binary solvent leads to two possible outcomes: i) the three-phase balance between precursor, gel solvent, and water cannot be achieved to obtain aerogels, and ii) the resulting aerogel exhibits larger particle size and higher density than the A3 aerogel (see Table S7, Supporting Information). Clearly, the structure and density of PDEMSEMVS aerogels can also be regulated by varying the ratio of binary solvents.

2.2. Mechanical and Thermal Insulating Properties

Owing to their nano-scale structures and chemical composition, the PDEMSEMVS aerogels have excellent mechanical properties and stability over a wide range of temperatures. Stress–strain curves and digital graphs of compression–decompression tests using a 500 g weight (**Figure** 4a,b) demonstrate the high compression flexibility of the optimized aerogels A3. These aerogels can undergo ≈75% strain without fracturing and fully recover their original shape after the removal of the 500 g weight. Furthermore, Figure 4c,d illustrates that the A3 aerogel maintains its structure even after undergoing 50 times compression-cycle tests at extreme temperatures of −80 °C, room temperature, or 200 °C, indicating potential applications in severe environments. This exceptional mechanical stability is attributed to the higher

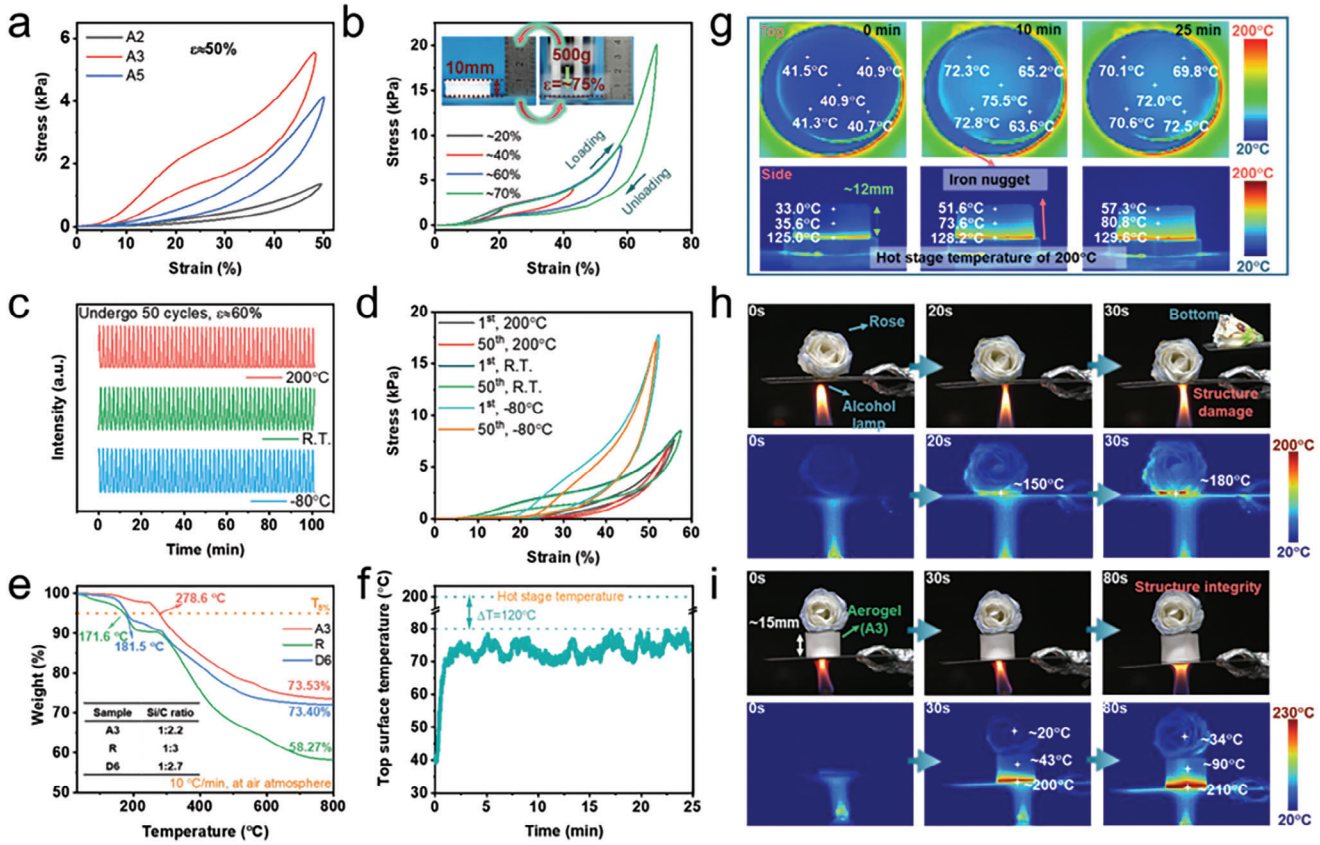

Figure 4. Physical property and thermal insulation performance. a) The compression stress–strain curves of various aerogels with 50% strain and b) of A3 aerogel with different strains (insect digital photos: aerogel compress-reply with 500 g weigh). c) The fatigue resistance test of A3 aerogel under different temperatures and d) corresponding stress–strain curves for 1st and 50th cycles. e) TG measure of A3 aerogel comparation to other organic silicone aerogel. f,g) The thermal insulation test of A3 aerogel under the 200 °C and h,i) further thermal insulation exhibition.

dissociation energy of the straight-chain Si—O bond (452 kJ mol^{-1}) compared to the C—C (346 kJ mol^{-1}), the greater length of Si—O bond (0.164 nm) compared to the C—C bond (0.154 nm), and the larger bond angle of the Si—O bond. Thus, the A3 aerogel can still be compressed to 50% strain and immediately recover its original size and shape when exposed to liquid N_2 at approximately −196 °C (Figure S10 and Movie S2, Supporting Information).

Further, the A3 aerogel possesses superior thermal stability compared to other aerogels reported due to its higher Si/C ratio (1:2.2) in the network.[23,26,39] For instance, the A3 aerogel exhibits a temperature of 5 wt% loss at 278.6 °C and 73.53% residual weight at 800 °C, compared to 181.5 °C and 73.40% for D6 and 171.6 °C and 58.27% for R (Figure 4e and Figure S11, Supporting Information). Additionally, Figure 4g, which shows optical images before and after exposure to a hot stage of 200 °C for 25 min, further confirms the high-temperature structural stability of the A3 sample. The A3 aerogel also shows a very low thermal conductivity, ~0.031 W m^{-1} K^{-1} (Table S7, Supporting Information), attributed to the micro-/nano-pore structure (Figure 3c). Importantly, the temperature of the top surface of the A3 aerogel sample placed on the 200 °C hot stage consistently remains a low temperature of <80 °C (Figure 4f). Moreover, the rose on the aerogel sample after being exposed on an alcohol burner maintained its structure stability when the sample thickness is ≈15 mm (Figure 4i and Movie S4, Supporting Information), while the control group experienced structural damage at the bottom (Figure 4h and Movie S3, Supporting Information). Notbaly, the A3 aerogel demonstrates superior thermal insulation properties when compared to other materials like melamine foam, silicone foam, and polyurethane foam (Figure S12, Supporting Information). This thermal insulating experiment underscores the potential of the proposed PDEMSEMVS aerogel for effective thermal management.

2.3. Super-Hydrophobicity and Oil/Water Separation Properties

As mentioned above, each aerogel demonstrates good surface hydrophobicity because of abundant hydrophobic groups in the aerogel network (Figure 2). Specifically, the PDEMSEMVS aerogel is surrounded by a dense air cushion and displays a sliver mirror-like surface when immersed in water, thanks to its water-repellent nanostructures that prevent the sagging of the liquid–air interface caused by the Laplace pressure[40] (**Figure 5**c). The contact angles of water on all the samples are greater than 150° (Figure 5a), and the roll-off angle of water is less than 6° (Figure 5a,b). Notably, the WCA of the A3 aerogel reaches an

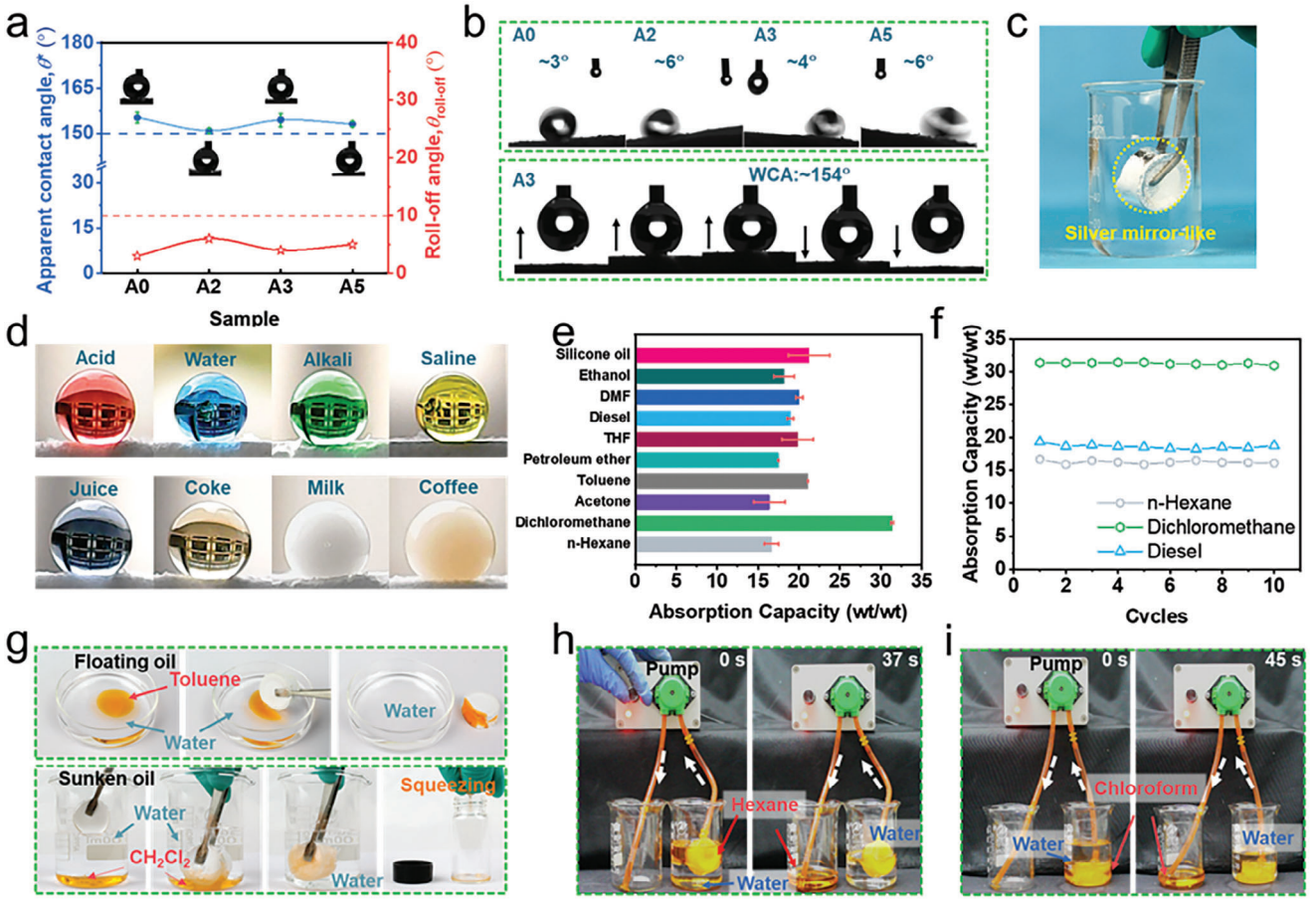

Figure 5. Superhydrophobic property and application of aerogels. a) Apparent contact angle (blue) and roll-off angle (red) of droplets on the various aerogels. b) And corresponding digital graphs of roll-off of aerogels and record of dynamic water droplet contact-depart experiment. c) Photograph of "silver mirror-like" aerogel and d) photographs of various liquids (e.g., acid (with Acid Red 6B), water (with $CuSO_4$), alkali (with $NiCl_2$), saline (with $K_2Cr_2O_7$), juice, coke, milk and coffee, 10 µL) on the A3 aerogel. e) Absorption capacities of A3 aerogel for various solvents and oils. f) Absorption/drying cyclic performance of A3 aerogel for *n*-hexane, dichloromethane, and diesel. g) The oil absorption process of the floating toluene and the underwater dichloromethane by using A3 aerogel. h,i) Photographs of continuous oil/water separation of hexane floating on the water surface and chloroform underwater using the oil collecting device.

impressive ≈154°, with a roll-off angle of less than 3° (Figure 5b). This remarkable behavior ensures that the water droplet does not infiltrate the aerogel, maintaining a super-hydrophobic state after landing 3 mL of the water droplet on its surface. These results confirm the outstanding super-hydrophobic properties of the PDEMSEMVS aerogels, which can be attributed to the abundance of the organic group (e.g., methyl and ethyl) with low surface energy in the molecules, as well as micro-scale pore cells containing nano-silicone particles within the 3D network framework of the aerogel.[40] Furthermore, for the acid, alkali, saline, juice, coke, milk, and coffee, the aerogel samples still kept excellent super-hydrophobicity (Figure 5d), indicating good water repellency for various water environments. As shown in Figure S13, Supporting Information, a nearly spherical water droplet forms on the PDEMSEMVS aerogel, while an oil droplet is immediately adsorbed by the block aerogel, implying the super-hydrophobic and super-oleophilic nature of the PDEMSEMVS aerogel surface.

Figure 5e illustrates that the A3 aerogel has a more than 15-fold solvent absorption capacity for various solutions including ethanol, *N*, *N*-dimethylformamide (DMF), tetrahydrofuran (THF), toluene, acetone, dichloromethane, petroleum ether, and *n*-hexane. Additionally, its absorption capacity for commercial oil, such as silicone oil and diesel, also can exceed 17 times the weight of the aerogel weight. Moreover, the A3 sample demonstrates stable absorption and cyclic drying performance, maintaining its high absorption capacity (>15 times) for *n*-hexane, diesel, and dichloromethane even after ten times absorption/drying process (Figure 5f), which further indicates its reliable and consistent oil–water separation efficiency. Furthermore, the A3 sample also exhibits impressive oil absorption from both the floating oil (e.g., toluene dyed by red Sudan) and sunken oil (e.g., CH_2Cl_2 dyed by red Sudan) in a static state (see Figure 5g and Movies S5 and S6, Supporting Information). Its lipophilic and hydrophobic properties enable the A3 aerogel to adsorb CH_2Cl from water and release and collect the oil without retaining water by squeezing the aerogel (Figure 5g). To evaluate the A3 aerogel's consecutive oil–water separation ability under dynamic conditions, an equipment is assembled to continuously collect oil spills in real-time from water by applying external pumping on the porous materials. The results, shown in Figure 5h,i and Movies S4 and S5, Supporting

Information, demonstrate that ≈30 mL of both the floating hexane (dyed by red Sudan) and the sinking chloroform (dyed by red Sudan) can be rapidly and continuously absorbed throughout the porous structure of the A3 aerogel in less than 45 s, and then pumped into a collecting empty beaker. These findings further confirm the efficient separation ability of the A3 aerogel.

2.4. How to Address the Gelation Issue in the Hydrosilylation Process?

It is important to note that the occurrence of gel formation, known as "free radical agglomeration," typically happens during the hydrosilylation reaction. This is evident in the absence of a peak corresponding to vinyl groups in the FTIR analysis (Figure S15a, Supporting Information). The gelation is attributed to the formation of free radicals (silyl radicals) that result from the transformation of Si—H functional groups in the presence of water and Pt catalyst.[41,42] Molecules containing multifunctional groups (such as vinyl), tend to undergo gelation and form insoluble gels in toluene (Figure S14a, Supporting Information) when free radicals are present in the reaction system. This phenomenon is less likely to occur with molecules that have monofunctional groups. Our analysis suggests that the presence of free radicals is caused by the presence of an H_2O molecule, possibly originating from the crystalline water in the chloroplatinic acid used in the preparation of the Karstedt catalyst. To address this issue, we introduced acetic anhydride, a water absorbent, in order to remove the H_2O molecule from the reaction system. This effectively controlled gel formation in the hydrosilylation process (Table S3, Supporting Information) and promoted the smooth progress of the graft reaction, with a conversion rate reaching 84.5%. It is important to note that acetic anhydride does not inhibit the Pt catalyst for the hydrosilylation process.[43] Additionally, the "Pt colloid", which combines Pt catalyst with O_2, can further promote the hydrosilylation process.[44] The resulting adducts with silane groups can dissolve in ethanol, forming a transparent solution (Figure S14b, Supporting Information), which is consistent with the chemical structure provided by the ^1H spectra (Figure S15b, Supporting Information). This strategy of using acetic anhydride to control gelation in the hydrosilylation between —CH=CH_2 and Si—H effectively restricts gelation in molecules with —CH=CH_2 functional groups. We have also employed this strategy in another reaction system in our subsequent experiments. Furthermore, the molecular weight of PMDS-vi and the amount of acetic anhydride may have an impact on the hydrosilylation reaction (Table S3, Supporting Information), which should be considered for further optimizing the structure of the polysiloxane aerogel.

3. Conclusion

In conclusion, we have successfully fabricated PDEMSEMVS wet gel, which contains long-straight chain Si—O—Si structures, using a consecutive graft-modified approach involving hydrosilylation and hydrolytic polycondensation. This approach enables the production of flexible aerogels with significantly lower density (≈50 mg cm^{-3}) compared to previously reported aerogels. Moreover, the resulting PDEMSEMVS-based aerogels exhibit a tunable size range (79 to 2800 nm) for their "silica particle." They also demonstrate super-hydrophobicity (water contact angle >150° and roll-off angle <6°), easy drying processability (under ambient temperature and pressure), outstanding compression resilience, excellent stability over a wide temperature range (−80 to 200 °C), multifunctionality including efficient absorption of organic solvents/oils and oil–water separation (with absorption capacities ranging from 16 to 31 g g^{-1}), and thermal conductivity of ∼31 mW m^{-1} K^{-1}. This novel approach provides a new series of flexible and ultra-low density aerogels that are well-suited for thermal insulation and oil/water separation.

4. Experimental Section

The detailed Experimental Section is provided in the Supporting Information.

Supporting Information

Supporting Information is available from the Wiley Online Library or from the author.

Acknowledgements

The authors acknowledge the funding support from the Natural Science Foundation of China (51973047 and 12002113), and the Science and Technology Key Project of Zhejiang Province (Z22E035302).

Conflict of Interest

The authors declare no conflict of interest.

Author Contributions

B.-F.G. and Y.-J.W. contributed equally to this work. B.-F.G.: Conceptualization, investigation, methodology, writing – original draft; Y.-J.W.: Methodology, investigation, writing – original draft. Z.-H.Q. and F.Y.: Methodology, investigation. Y.-Q. Q. and Y.L.: Methodology, software. G.-D.Z., J.-F.G., Y.S., and P.S.: Supervision. L.-C.T.: Writing – review & editing, funding support.

Data Availability Statement

The data that support the findings of this study are available from the corresponding author upon reasonable request.

Keywords

aerogel, hydrosilylation, micro-/nano-structure, polymer, superhydrophobic

Received: October 13, 2023
Revised: November 5, 2023
Published online: November 21, 2023

[1] W. Sakuma, S. Yamasaki, S. Fujisawa, T. Kodama, J. Shiomi, K. Kanamori, T. Saito, *ACS Nano* **2021**, *15*, 1436.
[2] B. Ren, J. Liu, Y. Rong, L. Wang, Y. Lu, X. Xi, J. Yang, *ACS Nano* **2019**, *13*, 11603.
[3] C. Xie, S. Liu, Q. Zhang, H. Ma, S. Yang, Z.-X. Guo, T. Qiu, X. Tuo, *ACS Nano* **2021**, *15*, 10000.
[4] Y. Si, J. Yu, X. Tang, J. Ge, B. Ding, *Nat. Commun.* **2014**, *5*, 5802.
[5] J.-Y. Hong, B. M. Bak, J. J. Wie, J. Kong, H. S. Park, *Adv. Funct. Mater.* **2015**, *25*, 1053.
[6] T. Bai, Y. Guo, D. Wang, H. Liu, G. Song, Y. Wang, Z. Guo, C. Liu, C. Shen, *J. Mater. Chem. A* **2021**, *9*, 5566.
[7] G. Zu, K. Kanamori, A. Maeno, H. Kaji, K. Nakanishi, *Angew. Chem., Int. Ed. Engl.* **2018**, *57*, 9722.
[8] S. Yang, J. Fan, S. Lin, Y. Wang, C. Liu, *Colloids Surf., A* **2020**, *585*, 124133.
[9] Z.-Y. Wu, C. Li, H.-W. Liang, Y.-N. Zhang, X. Wang, J.-F. Chen, S.-H. Yu, *Sci. Rep.* **2014**, *4*, 4079.
[10] J. Wang, D. Yuan, P. Hu, Y. Wang, J. Wang, Q. Li, *Adv. Funct. Mater.* **2023**, *33*, 2300441.
[11] A. Shimojima, K. Kuroda, *Chem. Rec.* **2006**, *6*, 53.
[12] G. Hayase, K. Kanamori, K. Nakanishi, *J. Mater. Chem.* **2011**, *21*, 17077.
[13] T. Kimura, T. Shimizu, K. Kanamori, A. Maeno, H. Kaji, K. Nakanishi, *Langmuir* **2017**, *33*, 13841.
[14] M. A. Hasan, R. Sangashetty, A. C. M. Esther, S. B. Patil, B. N. Sherikar, A. Dey, *J. Inst. Eng. (India): Ser. D* **2017**, *98*, 297.
[15] B. M. Novak, D. Auerbach, C. Verrier, *Chem. Mater.* **1994**, *6*, 282.
[16] S. Zhao, G. Siqueira, S. Drdova, D. Norris, C. Ubert, A. Bonnin, S. Galmarini, M. Ganobjak, Z. Pan, S. Brunner, G. Nyström, J. Wang, M. M. Koebel, W. J. Malfait, *Nature* **2020**, *584*, 387.
[17] A. V. Rao, *J. Porous Mater.* **2003**, *10*, 23.
[18] A. V. Rao, R. R. Kalesh, *J. Sol-Gel Sci. Technol.* **2004**, *30*, 141.
[19] X. Zhang, Y. Lei, C. Li, G. Sun, B. You, *Adv. Funct. Mater.* **2022**, *32*, 2110830.
[20] S. Takeshita, T. Ono, *Angew. Chem., Int. Ed.* **2023**, *62*, e202306518.
[21] L. Li, T. Hu, Y. Yang, J. Zhang, *J. Colloid Interface Sci.* **2019**, *540*, 554.
[22] L. Wang, R. Guo, J. Ren, G. Song, G. Chen, Z. Zhou, Q. Li, *Ceram. Int.* **2020**, *46*, 10362.
[23] G. Zu, T. Shimizu, K. Kanamori, Y. Zhu, A. Maeno, H. Kaji, J. Shen, K. Nakanishi, *ACS Nano* **2018**, *12*, 521.
[24] Z. Wang, Z. Dai, J. Wu, N. Zhao, J. Xu, *Adv. Mater.* **2013**, *25*, 4494.
[25] G. Zu, K. Kanamori, X. Wang, K. Nakanishi, J. Shen, *Chem. Mater.* **2020**, *32*, 1595.
[26] G. Hayase, K. Kanamori, M. Fukuchi, H. Kaji, K. Nakanishi, *Angew. Chem., Int. Ed. Engl.* **2013**, *52*, 2040.
[27] G. Hayase, K. Kugimiya, M. Ogawa, Y. Kodera, K. Kanamori, K. Nakanishi, *J. Mater. Chem. A* **2014**, *2*, 6525.
[28] Q. Wu, Q. Zhang, L. Zhao, S.-N. Li, L.-B. Wu, J.-X. Jiang, L.-C. Tang, *J. Hazard. Mater.* **2017**, *336*, 222.
[29] Q. Wu, L.-X. Gong, Y. Li, C.-F. Cao, L.-C. Tang, L. Wu, L. Zhao, G.-D. Zhang, S.-N. Li, J. Gao, Y. Li, Y.-W. Mai, *ACS Nano* **2018**, *12*, 416.
[30] H.-Y. Chen, Z.-Y. Chen, M. Mao, Y.-Y. Wu, F. Yang, L.-X. Gong, L. Zhao, C.-F. Cao, P. Song, J.-F. Gao, G.-D. Zhang, Y.-Q. Shi, K. Cao, L.-C. Tang, *Adv. Funct. Mater.* **2023**, 2304927.
[31] P. Meti, D. B. Mahadik, K.-Y. Lee, Q. Wang, K. Kanamori, Y.-D. Gong, H.-H. Park, *Mater. Des.* **2022**, *222*, 111091.
[32] T. Pirzada, Z. Ashrafi, W. Xie, S. A. Khan, *Adv. Funct. Mater.* **2019**, *30*, 1907359.
[33] J. Schraml, V. Chvalovský, M. Mägi, E. Lippmaa, *Collect. Czech. Chem. Commun.* **1977**, *42*, 306.
[34] E. A. Williams, J. D. Cargioli, S. Y. Hobbs, *Macromolecules* **1977**, *10*, 782.
[35] Y. Israëli, J. Lacoste, J. Cavezzan, J. Lemaire, *Polym. Degrad. Stab.* **1993**, *42*, 267.
[36] J. Schraml, Nguyen-Duc-Chuy, V. Chvalovský, M. Mägi, E. Lippmaa, *J. Organomet. Chem.* **1973**, *51*, C5.
[37] J. Soucek, G. Engelhardt, K. Stránský, J. Schraml, *Collect. Czech. Chem. Commun.* **1976**, *41*, 234.
[38] D. Khedaioui, C. Boisson, F. D'agosto, D. Montarnal, *Angew. Chem., Int. Ed.* **2019**, *58*, 15883.
[39] Y.-X. Qu, K.-Y. Guo, H.-T. Pan, Z.-H. Wu, B.-F. Guo, X.-L. Feng, T.-T. Kong, C. Zhang, G.-D. Zhang, L. Zhao, L.-X. Gong, J.-F. Gao, H.-L. Liu, Z.-N. Mao, L.-C. Tang, *Mater. Today Chem.* **2022**, *26*, 101068.
[40] D. Wang, Q. Sun, M. J. Hokkanen, C. Zhang, F.-Y. Lin, Q. Liu, S.-P. Zhu, T. Zhou, Q. Chang, B. He, Q. Zhou, L. Chen, Z. Wang, R. H. A. Ras, X. Deng, *Nature* **2020**, *582*, 55.
[41] P. Hu, J. Madsen, A. L. Skov, *Nat. Commun.* **2022**, *13*, 370.
[42] Z. Yang, M. Iqbal, A. R. Dobbie, J. G. C. Veinot, *J. Am. Chem. Soc.* **2013**, *135*, 17595.
[43] K. Manabe, S. Kobayashi, *Org. Lett.* **2003**, *5*, 3241.
[44] L. N. Lewis, R. J. Uriarte, *Organometallics* **1990**, *9*, 621.